Journal of Analytical and Applied Pyrolysis 169 (2023) 105820

Contents lists available at ScienceDirect

Journal of Analytical and Applied Pyrolysis

journal homepage: www.elsevier.com/locate/jaap

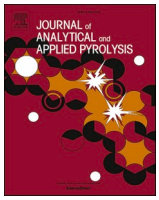

Analysis and distribution of volatile gases from catalytic pyrolysis of Sulcis low-rank coal

Silvera Scaccia

(TERIN-PSU-IPSE), C.R. ENEA, Casaccia, V. Anguillarese 301, I-00123 Rome, Italy

A R T I C L E I N F O

Keywords:
Catalytic pyrolysis
Sulcis low-rank coal
Olivine and Ni/γ-Al_2O_3 catalyst
Quantitative gas distribution
Isoconversional method

A B S T R A C T

Catalytic pyrolysis of Sulcis low-rank coal over naturally occurring olivine, and home-made 15 wt%Ni/γ-Al_2O_3 catalyst was conducted for the upgrading of coal pyrolysis volatile gases in the temperature range ambient-900 °C under atmospheric pressure. Raw coal and mixtures of coal-additive (90:10 wt%) were slowly heated in temperature programmed mode using a laboratory-scale quartz furnace coupled in parallel to Fourier transform infrared (FTIR) spectrometer and GC chromatograph for quantitative analysis of flue gas. Coal pyrolysis with and without additives was also conducted by TG/DTG/DSC analysis at different heating rate (β = 15, 20, 30 °Cmin^{-1}). DSC results clearly indicated some extra exothermic events during catalytic coal pyrolysis. Quantitative gaseous products distribution with temperature showed yields significantly and selectively improved with additives. Generally, more CO and CO_2 were emitted under catalytic coal pyrolysis. Meanwhile, nickel catalyst exerted a marked positive effect on H_2 yield overall in the temperature range 400–500 °C. The light hydrocarbons such as methane, ethane, propane and n-hexane substantially remaining unchanged, whereas a remarkable increase of emitted ethene was originated from catalytic pyrolysis. A deeper SO_2 evolution was observed over olivine, whereas the N-containing compounds (NH_3, NO_x) were also modified in catalytic pyrolysis. Formaldehyde was also monitored, which represents a fragment originating from polycyclic aromatic side chains. Reaction kinetic study by a model-free isoconversional method indicated a complex multiple-step mechanism of coal pyrolysis, exception made for conversion values between 5% and 50% where a single-step reaction path was operating. The calculated average E_a and the pre-exponential factor were markedly reduced by the presence of additives. Meanwhile the compensation effect was also existing.

1. Introduction

Pyrolysis is a well-known efficient and environmentally benign technology, which allows to transform organic carbonaceous matter into permanent gases and valuable liquid fuels by means of heating at relatively low temperature under oxygen-free atmosphere, whereas a valid solid feedstock (char) is produced. Pyrolysis is the initial stage common to all the thermo-chemical conversion processes of coal (combustion, gasification, and/or oxy-combustion) for energy production [1]. It is well-established that coal pyrolysis process can be sketchily divided into two stages: the first stage is devolatilization during which fragmentation of organic macromolecules, referred as TAR, and primary reactions take place; and the second one is reforming of volatiles and secondary reactions [2]. However, to upgrade TAR into lighter one and available gaseous products (mainly H_2 and CO) for commercial applications, more deeply identification of thermal degradation reactions and product distribution taking place during coal pyrolysis should be made from both a qualitative and quantitative point of view [3].

Because the pyrolysis process is greatly affected by the type of coal rank, particle size, heating rate, residence time, catalysts and so on, a relevant influence on subsequent steps of thermal processing is recognized [4]. Specifically, to obtain a good quality of pyrolytic gases proper catalysts are employed in coal pyrolysis both in-situ for TAR cracking and *in series* for the upgrading of generated volatiles and gasification reactions of char [5,6].

In catalytic coal pyrolysis a wide number of catalysts has been employed from naturally occurring minerals such as olivine (mixed iron, magnesium, and silicon oxides) and dolomite (double magnesium calcium oxide) to nickel-based catalyst. It is well established that coal contains inherent inorganic materials having catalytic effect on the conversion of organic matter during low temperature thermo-chemical processes [7]. Iron oxides and CaO can act as catalysts notably enhancing methane production [8,9]. Olivine and dolomite have been used as catalyst/bed material for TAR cracking-reforming/heat carrier

E-mail address: silvera.scaccia@enea.it.

https://doi.org/10.1016/j.jaap.2022.105820
Received 19 October 2022; Received in revised form 23 November 2022; Accepted 2 December 2022
Available online 6 December 2022

[10,11]. Although the olivine catalytic activity towards TAR decomposition is lower than dolomite, it presents superior mechanical strength over dolomite, which generates owing to elutriation more fines and particulates in the flue gas [12]. Moreover, olivine has been used as catalyst in methane and tar steam reforming [13], and tar cracking [14]. The superior catalytic capability of metallic iron over iron oxides was stated in various investigation on crack tar in biomass [15]. Iron as metal is more effective to crack C-C and C-O bonds in tar biomass compared to iron oxides [16,17].

Nickel-based catalysts have excellent metallic species for steam gasification/reforming reactions and are preferred as catalytic active sites, even at low temperatures of 450− 500 °C, compared to precious metal such as Pt, Ru, and Rh, because of the low cost and abundance [18–20]. Nickel-based catalysts are often used in pyrolysis and catalytic up grading of low rank coal [21–23]. In particular, the nickel catalysts supported over Al_2O_3 have been extensively employed in reforming and cracking of light hydrocarbons for producing H_2-rich gas [24,25]. Moreover, the Al_2O_3 support are often used in catalytic cracking process owing to its good thermal/hydrothermal stability and high mechanical strength [26,27]. However, nickel catalyst deactivation by excessive coke deposition or sulphur inhibition can limit its use. These drawbacks could be overcome by catalytic cracking with steam, which is a milder and more favourable condition to avoid deactivation of the catalyst [28]. Moreover, the in situ catalytic coal pyrolysis over nickel-based catalysts presents some unique advantages in the conversion of TAR owing to their strong catalytic activity [29–32]. Indeed, the use of nickel catalyst during the coal pyrolysis could improve the yield of emitted gases such as light hydrocarbons and H_2 via decomposition of macromolecules and polydecondensation of aromatics in low rank coal [33]. After gasification/combustion, spent olivine can be used as bed material, while spent NiALO along with residual ash can be regenerated because the ash contains inherent inorganic oxides such as Al_2O_3, Fe_2O_3 etc., which have good catalytic activity or can be used as a carrier for the Ni catalyst.

In previous works [34,35], the pyrolysis of low rank coal from Sulcis area (Sardinia, Italy) was investigated in thermogravimetric analyser and in fixed-bed reactor type coupled to FTIR technique for the analysis of evolved gases in a qualitative manner. In the present work the non-catalytic and catalytic pyrolysis of low rank Sulcis coal over naturally occurring olivine and a home-made 15 wt%Ni/γ-Al_2O_3 catalyst was investigated in a fixed-bed reactor-type heated up to 900 °C under N_2-atmospheric pressure and simultaneously coupled to FTIR spectrometric and GC chromatographic analysers. The distribution patterns of gaseous products were evaluated in a quantitative manner. The kinetic parameters for non-catalytic and catalytic coal pyrolysis were also evaluated by a model-free isoconversional method from TG data. The gathered results will shed some new insights over the primary volatile compositions and formation mechanisms during catalytic coal pyrolysis.

2. Experimental

2.1. Samples

The low-rank coal sample was collected from Sulcis field, Sardinia, Italy. The bulk coal sample was crushed by means of a jaw crusher and ground in a ball mill to give fractions of mean particle size lower than 100 μm as measured by scanning electronic microscopy. Proximate analysis of raw coal was carried out according to the ASTM E1131 Test method by instrumental procedures. Ultimate analyses of raw coal and chars were conducted by a C/H/N/and sulfur elemental analyzer (LECO TruSpec) according to ASTM D 5373–08 and ASTM D 4239–08 Test method. All the results are given in Table 1.

Natural mineral olivine was from quarry of Biella (Italy), a locality in the foothills of Alps. Olivine had a mean particle size of $500{\cdot}10^{-6}$ m and apparent density of 2300 kg·m^{-3}. XRD analysis (not showed here) confirmed the composition of pristine olivine as a solid solution of magnesium and iron silicate. Owing to the difficult in detecting free-iron oxides on olivine's surface by XRD, temperature programmed reduction (H_2-TPR) was conducted on olivine as described in [31]. The H_2-TPR profile of olivine shown in Fig. 1 displayed several reduction peaks between 150 and 800 °C attributable to reduction of free-iron oxides in olivine ($FeOOH \rightarrow Fe_2O_3 \rightarrow Fe_3O_4 \rightarrow FeO \rightarrow Fe$) in accordance with literature data [36,37].

Table 1
Proximate and ultimate analysis results of raw Sulcis coal.

Proximate	Moisture	Volatile Matter	Fixed Carbon	Ash	
wt%	5	39	43	13	
Ultimate	**C**	**H**	**N**	**S**	**O**[a]
wt% (dry basis)	58	4.6	1.6	6.0	16.8

[a] Oxygen content calculated by difference method: [O]= 100-[C]-[H]-[N]-[S]-[ash].

Home-made 15 wt%Ni/γ-Al_2O_3 catalyst, denoted as NiALO, was prepared and characterized as detailed described elsewhere [38]. Thermal stability of additives was investigated by TGA from room temperature to 900 °C under the pyrolysis conditions. No significant weight loss was founded for both olivine and NiALO, indicating that they possess high stability.

2.2. Preparation of mixtures of coal/ additive

Raw coal powder and additive (olivine and NiALO) in the weight ratio 9:1 was mixed with 2-propanol by wet-mixing method for 5 h. Then, the slurries were dried at 120 °C for 2 h. The obtained mixtures were then stored in dessicator before use.

2.3. Thermogravimetric analysis

Thermogravimetric(TG)/derivative theromagravimetric(DTG/differential scanning calorimetry (DSC) analyses were accomplished in a TGA/DSC1 STARe System (Mettler-Toledo, Switzerland). The sample mass was placed in open cylindrical alumina crucibles ($30{\cdot}10^{-6}$ L). Nitrogen (99.99%, Air Liquid, France) was used as the purge gas at 0.030 L min^{-1} to protect the balance. Typical sample mass of 0.015 g was heated from room temperature to 900 °C at 15, 20, and 30 °C min^{-1} heating rates under N_2 atmospheres at 0.17 L min^{-1} flow rate. The total flow rate was 0.20 Lmin^{-1}. Blank correction runs were carried out to minimize the Buoyancy effect. The TG runs were repeated at least twice.

2.4. Temperature-programmed pyrolysis test

Non-catalytic and catalytic pyrolysis of Sulcis coal was conducted by the bench scale setup schematically illustrated in Fig. 2. Briefly, 5 g of

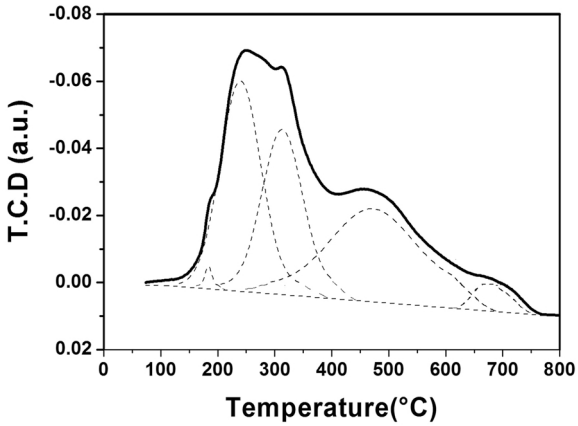

Fig. 1. H_2-TPR profile (—) and deconvoluted peaks (- -) of natural olivine.

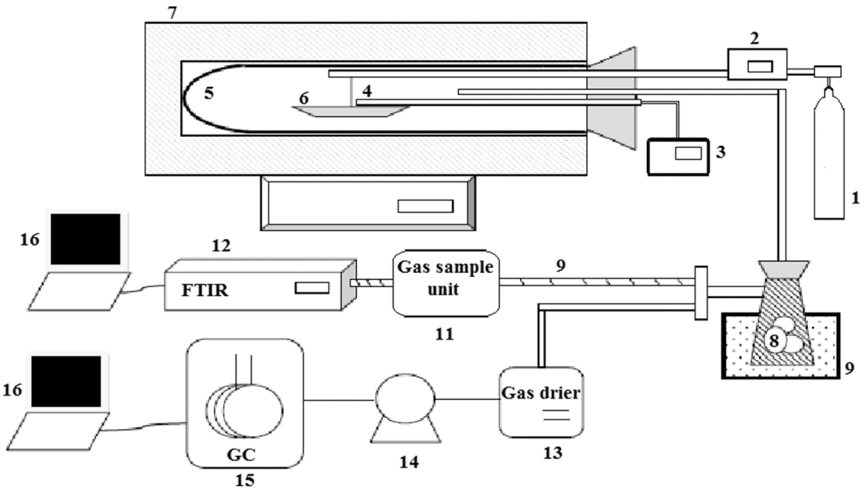

Fig. 2. Schematic diagram of apparatus for non-catalytic/catalytic coal pyrolysis. (1) N_2 gas cylinder. (2) Mass flow controller. (3) Temperature controller. (4) Thermocouple. (5) Reactor. (6) Alumina boat. (7) Electric furnace. (8) Cotton wool. (9) Cold bath. (10) Heated transfer line. (11) Gas sampling unit. (12) FTIR. (13) Gas drier. (14) Sampling pump. (15) GC. (16) PC.

mixture of coal/inert quartz wool, coal/olivine and coal/Ni catalyst were loaded on an open-alumina boat hanging from a stainless steel rod and placed in the middle of a quartz tube reactor (30 mm in diameter and 250 mm in length), which was located in an horizontal electric furnace. A K-type thermocouple was inserted for online monitoring sample temperature. The N_2 carrier gas (99.99% purity, Air Liquid) was regulated at 0.2 $Lmin^{-1}$ flow rate trough a mass flow controller (EL-FLOW, Bronkhorst High Tech®). Before the start of each pyrolysis run the quartz-tube reactor was purged with N_2 for 30 min to ensure an inert atmosphere. The sample was heated from room temperature to 900 °C at 15 °$Cmin^{-1}$ heating rate. The liquid product (TAR+water) was trapped in a quartz flask containing cotton wool, which was immersed in a nitrogen liquid-2-propanol azeotropic mixture (−30 °C). The pure volatile gas was continuously sent both to the Gasmet DX-4000 FTIR through a heated transfer line and the GC, which were set in parallel to the cold trap for the online gas analysis as described in the below sections. Triplicates runs were conducted to verify the reproducibility of entire set-up. The results were given as dry-free (df) basis. TAR yield was calculated as reported in [29]. The TAR yields were 14.0, 13.1, and 12.7 for non catalytic and catalytic coal pyrolysis over olivine and Ni/ALO, respectively.

2.5. Analytical instrumentation for the analysis of gases

Agilent 6850 gas chromatograph-TCD detector equipped with two columns connected in series, namely, Molesieve 5 A for permanent gases (H_2, N_2, O_2, CO, and CH_4) and Hayesep Q for CO_2 was used was used. Quantification was made by GC Chemstation software (Agilent) according to the predefined method. The GC was calibrated with reference gas (Air Liquid, France) supplied by high pressure cylinders before the start and after the end of carbonation test. The ratio between sample peak area and the bracketing reference peaks is used to calculate gas volume %.

Gasmet DX-4000 portable multicomponent gas analyser, incorporating a low-resolution (4 cm^{-1}) Fourier transform infrared spectrometer and a ZrO_2 sensor for accurate O_2 measurements, was used to determine gaseous components of coal pyrolysis gas. It was equipped with a temperature-controlled gas cell, heated transfer line, and gas sampling unit for gas sampling and cleaning. CALCMET software was used, which analyzes the acquired sample spectrum using a sophisticated algorithm. The software can simultaneously detect, identify, and quantify of up to 50 different gas components from a single sample. Cross-interference effects are compensated for and the analysis accuracy is maintained even when analyzing complex gas mixtures where gases have overlapping absorption spectra [39]. The precise band assignments are given in Table 2. The DX4000 instrument was factory calibrated and typically was set up to measure evolved gases such as CO_2 (0–80% v/v), CO (0–2000 $mgN^{-1}m^{-3}$), CH_4 (methane, 0–1000 $mgN^{-1}m^{-3}$), C_2H_6 (ethane, 0–1000 $mgN^{-1}m^{-3}$), C_3H_8 (propane, 0–1000 $mgN^{-1}m^{-3}$), and C_6H_{14} (n-hexane, 0–1000$mgN^{-1}m^{-3}$), C_2H_4 (ethene) (0–200 $mgN^{-1}m^{-3}$), SO_2 (0–2000 $mgN^{-1}m^{-3}$), NO_2 (0–200 $mgN^{-1}m^{-3}$), NO (0–50 $mgN^{-1}m^{-3}$), NH_3 (0–100 $mgN^{-1}m^{-3}$), and CH_2O (formaldehyde, 0–50 $mgN^{-1}m^{-3}$) with 2% error. FTIR spectra were also collected and stored on the hard disk of analyser along with the concentration information to check possible spectral overlapping. The obtained spectra and the concentrations of the gases were handled and further determined with Calcmet Software. The dynamic evolution of the emitted gases from coal pyrolysis were constructed as concentration measured at a given characteristic band of each gaseous species versus temperature. Otherwise stated, the curves were also deconvoluted by Gaussian-type function and peak fitting (Origin Pro 8 software).

3. Results and discussion

3.1. Qualitative and quantitative analysis of volatiles gases

The typical FTIR spectra of gaseous products taken at different temperatures during non-catalytic and catalytic N_2-pyrolysis of Sulcis coal in programmed temperature quartz fixed-bed reactor are depicted in Fig. 3. As can be seen from Fig. 3 Sulcis coal pyrolysis with and without additives generates predominantly gaseous products including CO_2, CO, light hydrocarbons, SO_2, NH_3, NO_x, and CH_2O (formaldehyde). This latter was monitored as example of generated fragment from organic matter. Among the light hydrocarbons CH_4, C_2H_6, C_3H_8, C_6H_{14}, and C_2H_4 were chosen for the analysis because depending on pyrolysis

Table 2
Band Assignment of FTIR Spectra during non-catalytic and catalytic coal pyrolysis.

Wavenumber (cm^{-1})	Assignment	Wavenumber (cm^{-1})	Assignment
2076	CO_2	2941	C_6H_{14}
2177	CO	1165	SO_2
3018	CH_4	964	NH_3
2981	C_2H_6	1629	NO_2
950	C_2H_4	1914	NO
1340	C_3H_8	2802	CH_2O

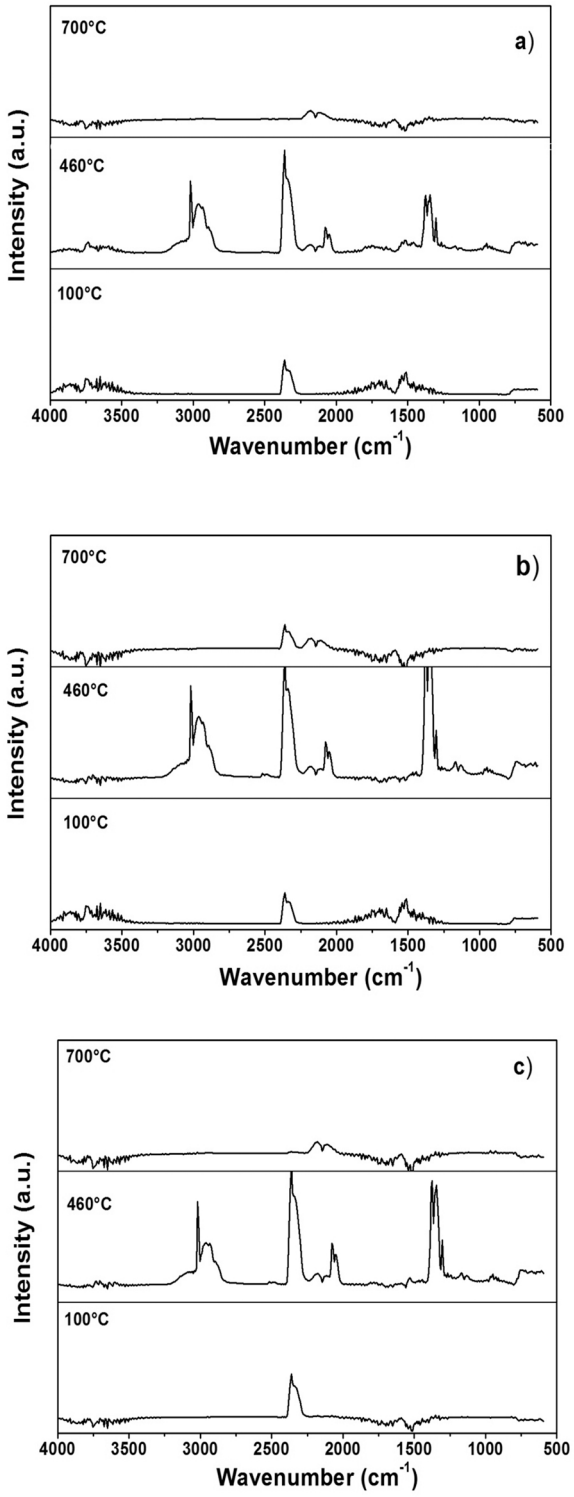

Fig. 3. FTIR spectra of evolution at different temperatures from non-catalytic pyrolysis (a) and catalytic pyrolysis of Sulcis coal over olivine (b) and NiALO catalyst (c).

conditions, the coal pyrolytic gas is mainly rich in these organic gases. The quantitative results of yielded pyrolytic gas composition are reported in Table 3. Meanwhile the H_2 results (not IR active) obtained by GC are also reported in Table 3. Interestingly, CO_2, CO, and CH_4 were also analyzed in parallel by GC and the results largely agreed with those obtained by FTIR analysis. Generally, the presence of both the mineral olivine and NiALO catalyst during coal pyrolysis induces a beneficial effect in producing higher content of gaseous products compared to non-catalytic coal pyrolysis. The dynamic temperature-concentration profiles of each gaseous species produced during the non-catalytic and catalytic pyrolysis of coal will be discussed below.

3.2. Evolution distribution of gases

3.2.1. CO_2, CO, and H_2

The temperature-concentration profiles of dominant gaseous products of CO_2, CO, and H_2 from non-catalytic and catalytic coal N_2-pyrolysis over olivine and NiALO catalyst are showed in Fig. 4(A-C). As can be seen from Fig. 4(A,a) the release of CO_2 was already observed in the initial stage of Sulcis low rank coal pyrolysis due to the thermal decomposition of oxygen-containing functional groups and/or CO_2 desorption from porous structure of coal [40,41]. With the temperature rising, various deconvoluted peaks of CO_2 emission appeared of up to 300 °C. Subsequently, a highly intense double CO_2 peak between 400 and 650 °C was emerged. Generally, the CO_2 evolution in the range 500–800 °C is influenced by the presence and content of oxocarbon (esters and quinones) and inherent inorganic carbonates [42]. In catalytic coal pyrolysis some extra CO_2 evolution peaks were identified (Fig. 4A,b-c). However, the catalytic effect of olivine on pyrolytic gas production was less effective than that of NiALO catalyst, exception for a peak around 700 °C, probably due to the reduction of Fe_3O_4/FeO through the nascent formed CO [8,43]. Coal pyrolysis over NiALO catalyst presented a remarkable enhancement of CO_2 emission in the entire range of temperature 50–400 °C. Usually, a significant increase of CO_2 volatilization catalysed by Fe and Ni metallic was often reported in literature, which was ascribed to cracking reactions of carboxylic groups in primary pyrolysis [44,45].

The representative temperature-concentration profiles of CO evolved from non-catalytic and catalytic pyrolysis are depicted in Fig. 4(B). The CO emissions were observed into two distinctly temperature zone: the first stage at low temperature between 150 and 500 °C was due to desorption of CO and/or breakage of weak bonds of oxygen-bearing heterocycles, ethers, ketones, and carboxyl group from aliphatic and aromatic carboxyl and carboxylate [46]. The second stage at high temperature between 500 and 900 °C produced a very large peak of CO evolution composed of two overlapping deconvolved peaks originating from secondary reactions of tar compounds. But for low rank coals the CO emission in this temperature range is also ascribed to in situ gasification (Boudouard's reaction) of the nascent char exposed to freshly formed CO_2 during coal pyrolysis as indicated by the concomitant rapid rate decay of CO_2 emissions [35]. Similar distribution pattern of CO evolution was observed for coal pyrolysis over olivine (Fig. 4Bb). Conversely, the addition of NiALO catalyst to raw coal induced a larger effect on coal thermal degradation at low temperature as CO release during pyrolysis continuously increased with the increasing of temperature, whereas solely one large CO emission peak was evolved in the second stage (Fig. 4Bc). It is supposed that nickel-based catalyst might catalyse cracking reaction of oxygen heterocycles [47].

The temperature-concentration curve of H_2 from non-catalytic coal pyrolysis (Fig. 4Ca) shows the beginning of evolution at about 500 °C with the maximum release rate at 700 − 800 °C, whose deconvolution peaks were at 578, 650 and 788 °C in agreement with literature data [48,49]. The molecular H_2 is originated at least from two reactions types: i) the predominantly maximum release of H_2 was attributed to radical polycondensation of aromatic ring, and ii) dehydrogenation reactions at high temperature [50,51]. In coals, owing to their high content of aromatic structures, aromatization and condensation reactions could be the preferential mechanism path for H_2 evolution [52]. Usually, H_2 release was accompanied by CO evolution due to secondary pyrolysis reactions at high temperature [53]. It is worthy to note that H_2 can also be generated through gasification of nascent char during pyrolysis by in situ formed steam gasification agent [54]. In coal carbonization with added olivine a similar evolution behaviour was observed (Fig.4Cb).

Table 3
Yield ($mgN^{-1}m^{-3}$) of non-condensable gases evolved from non-catalytic and catalytic Sulcis coal N_2-pyrolysis.

	CO_2	CO	H_2	CH_4	C_2H_6	C_3H_8	C_6H_{14}	C_2H_4	CH_2O	SO_2	NH_3	NO_2	NO
Sample													
Coal	1418	900	1248	413	255	123	218	24	4	776	52	195	29
Coal/olivine	2365	1229	1347	389	226	109	163	52	8	1260	15	155	9
Coal/NiALO	2481	1060	1900	403	241	109	180	59	5	1260	19	135	22

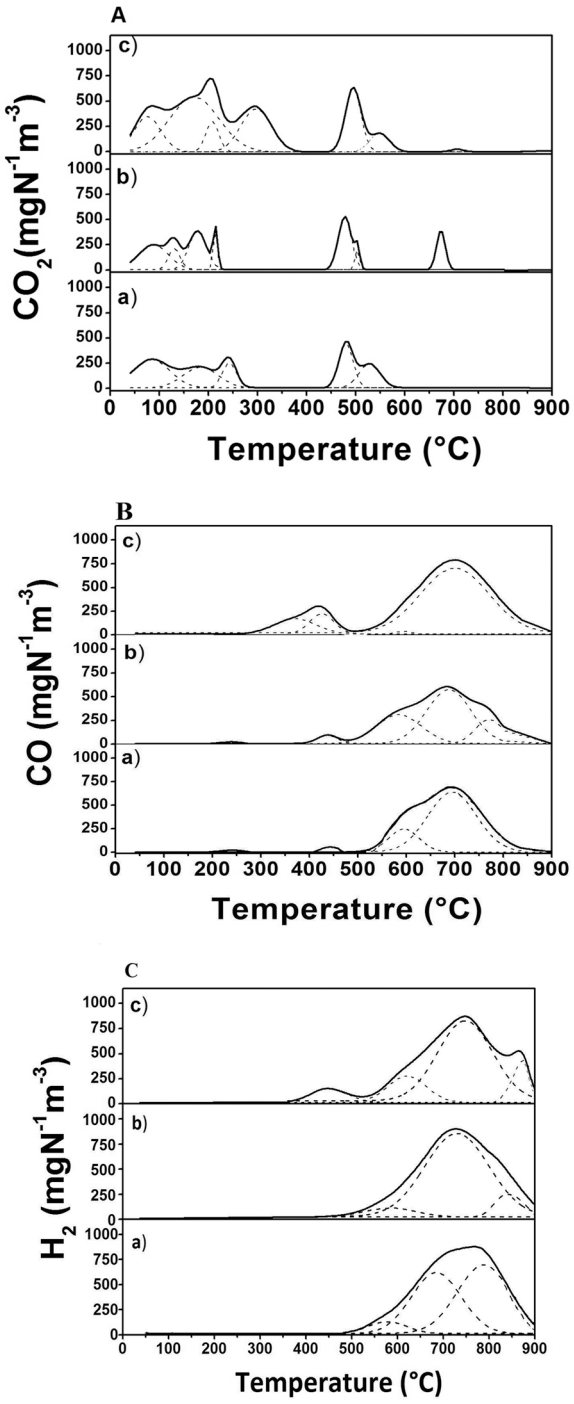

Fig. 4. CO_2 (A), CO (B), and H_2 (C) evolution/deconvoluted curves during non-catalytic pyrolysis (a) and catalytic pyrolysis of Sulcis coal over olivine (b) and NiALO catalyst (c).

Differently, in presence of NiALO catalyst the appearance of H_2 evolution begins at temperature as low as 300 °C and proceeded up to 900 °C (Fig 0.4 Cc). Deconvolution of H_2 emission curve showed four deconvolved peaks centred at 450, 500, 650, and 750 °C. The first smaller H_2 evolved peak might derivate from catalytic cracking of aliphatic. However, at temperature below 500 °C some secondary reactions such as char gasification and water gas shift reactions, which are catalysed by both the metallic nickel and iron, might also take place through CO_2 and pyrolytic water consumption as described below [55,56]:

$$Ni + CO_2 \leftrightarrow NiO + CO \quad (1)$$

$$Ni + H_2O \leftrightarrow NiO + H_2 \quad (2)$$

3.2.2. *Alkanes (C_1-C_3, C_6), alkene ($C_{2=}$) and formaldehyde (CH_2O)*

The overall distributions of light gaseous hydrocarbons, including both alkanes (methane, ethane, propane, and hexane) and alkene (ethene), as a function of the temperature during non-catalytic and catalytic coal pyrolysis are depicted in Fig. 5. Methane was the most abundant product yield among all the aliphatic carbon, which appearance temperature occurred at approximately 270 °C and ended at 800 °C with maximum release rate around 540 °C (Fig. 5A). Generally, it is recognized that methane formation under coal pyrolysis occurs through the breakage of aryl/alkyl-ether bonds and methyl side chains that subsequently are hydrogenated [2,57]. All other alkanes presented similar nearly Gaussian distribution, which was extending in a narrower range of temperature between 300 and 700 °C (Fig. 5A). However, the addition of both olivine and NiALO catalyst to coal during pyrolysis has little effect on the yield and emissions of saturated hydrocarbons. Small molecules of hydrocarbons could be trapped in raw coal and volatilize on heating depending on coal rank and operating conditions [58]. Meanwhile it is supposed that light hydrocarbons C_{2+} can derive from thermal cracking reactions of aliphatic side chains of coal matrix and/or liquid hydrocarbons [59,60]. On the contrary, the pyrolytic evolution of the n-alkene such as ethene was remarkably enhanced under catalytic pyrolysis of coal (Fig. 5B). It was reported that n-alkenes are predominantly derived by thermolysis of long alkyl-aryl structures [61]. Nickel catalysts was able to catalyze cracking reactions of light hydrocarbons with formation of small hydrocarbons such as ethene and H_2 [62]. Meanwhile the CH_4 originating from scissions of long-chain alkanes bonds can be activated to form $CH_3^{\bullet}$ free-radicals, which dimerize to form alkene compounds with H_2 by-products [63]. However, the presence of Fe_2O_3 additive favors the production of alkenes with short chains through cracking reactions of polycondensate matter [43,64].

The temperature-concentration curves along with the deconvoluted curves of formaldehyde (CH_2O) during the whole process of non-catalytic and catalytic Sulcis coal pyrolysis are showed in Fig. 5(C). The formaldehyde compound can be considered as a volatile fragment generated through the cleavage of C-C bonds in alkyl side chains containing –CH_2OH or carboxylic groups in primary thermal degradation [65,66]. The CH_2O emitted distribution was over the temperature range 200–800 °C, which presented three main deconvoluted peaks at 298, 420, and 490 °C. Except is made for the catalytic pyrolysis over natural olivine, which showed two extra peaks of emission at 240 and 620 °C. This indicates that the presence olivine has a significant influence on degradation of macromolecules into small molecules as volatiles. It is

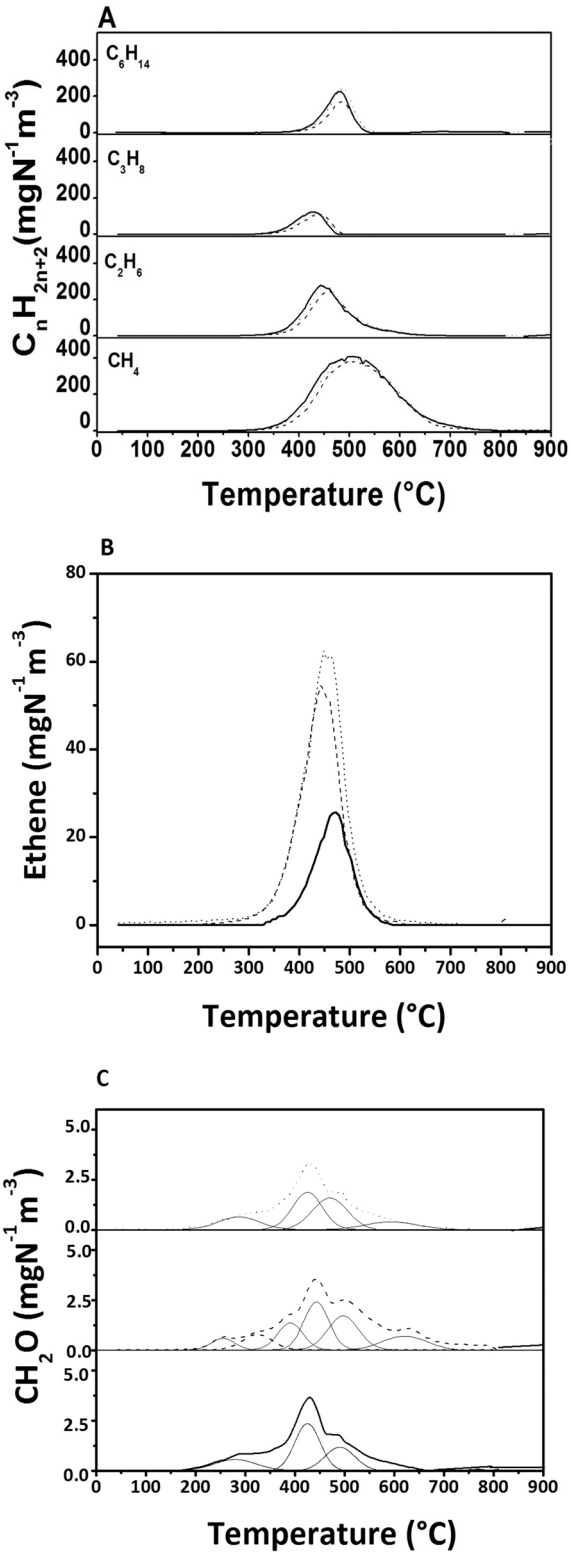

Fig. 5. Alkanes (A), alkene (B), and CH_2O (C) evolution/deconvolved curves during non-catalytic (-) and catalytic pyrolysis of Sulcis coal over olivine (–) and NiALO (··).

probably that metallic iron mostly produced by reaction of free-iron oxides in olivine surface with reducing coal pyrolysis gases have a more effect on tar degradation [67].

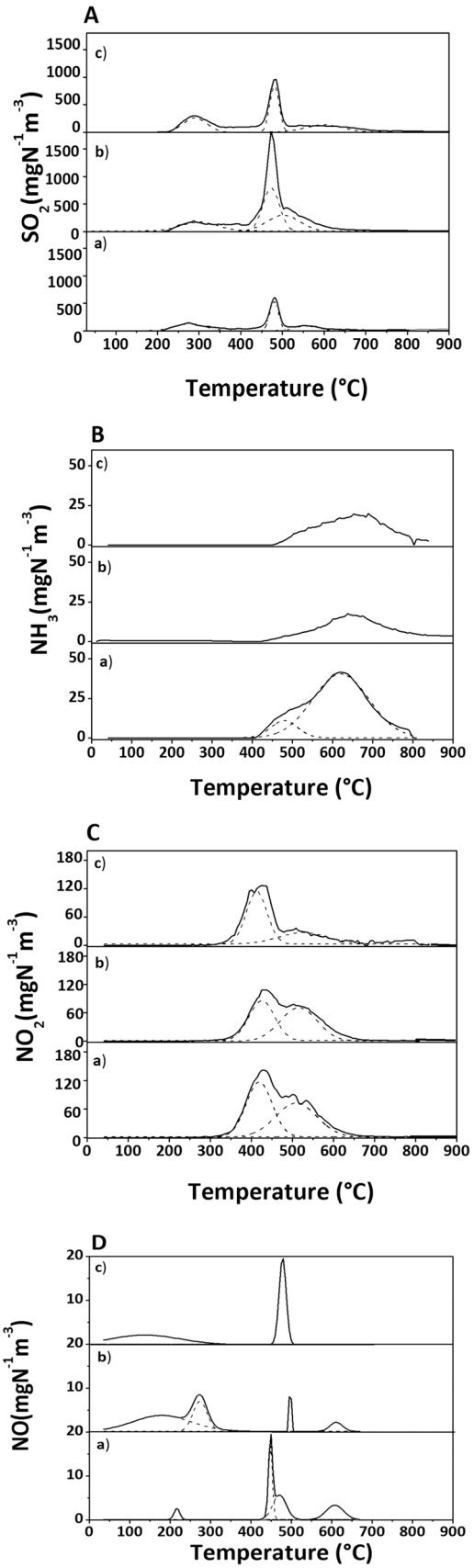

Fig. 6. SO_2 (A), NH_3 (B), NO_2 (C), and NO (D) evolution curves during non-catalytic pyrolysis (a) and catalytic pyrolysis of Sulcis coal over olivine (b) and NiALO catalyst (c).

3.2.3. SO_2, NH_3, NO_2, and NO

The SO_2 temperature-evolved profiles exhibited during the whole process of non-catalytic and catalytic Sulcis coal pyrolysis are shown in Fig. 6(A). The evolution profiles were substantially similar, even though the yield was significantly larger when using natural olivine additive (Table4). Deconvolution of temperature-emission curves showed three main peaks at approximately temperature of 300, 500 and 600 °C (Fig.6Aa). It was well established in the literature that SO_2 evolution from coal N_2-pyrolysis has different sulphur origins, although the mechanisms of formation were not yet well understood. The inherent inorganic matter in coal can play a key factor in organic/inorganic sulphur retention in char structure [68]. Sulphur dioxide starts to emit at low temperature (250–350 °C) owing to displacement of labile organic sulfonic acid group decomposition [69]. In coal-containing pyrite the SO_2 evolution can come from iron sulphate decomposition [70]. In combustion conditions FeS_2 decomposes to SO_2 and Fe_2O_3 at 500 °C, whereas in oxygen-free atmosphere can be formed FeS and S, the latter undergoing to oxidation by O-char to SO_2 [71]. Secondary reaction of $^{\bullet}$SH radical formed during pyrolysis at higher temperature with nascent char was also responsible of SO_2 [72]. The enhanced catalytic effect of natural olivine on tar cracking was overall ascribed to the presence of iron oxides/metallic iron dispersed onto the surface of olivine (Fig.6Ab). Owing to the oxygen-carrier properties of olivine more SO_2 can be formed from FeS_2 or/and F_2S at temperature below 500 °C in concomitance with the reduction of iron oxides to FeO, which is a better catalyst for tar removal [10]. Fig.6Ac shows as the enhanced evolution of SO_2 at low temperature may be related to the concomitant increasing of CO_2 emission in presence of nickel catalyst. It was reported the coal sulphur conversion into gaseous sulphur in tar and volatile is favoured in CO_2 atmosphere, whereas the decomposition of sulphates at high temperatures is also promoted [73].

The temperature-concentration profiles of NH_3, which is a precursor of NO_x species under oxidation conditions, from non-catalytic and catalytic coal pyrolysis is depicted in Fig. 6(B). From Fig. 6(B) it can be seen the emission profile of NH_3 from coal pyrolysis without additive showed two overlapped peaks at around 500 and 650 °C. The formation of NH_3 from coal pyrolysis is supposed of coming from NH_3 group liberation of N-containing tar or secondary reactions between nascent free $H^{\bullet}$ radical and N-containing char [74]. Catalytic coal pyrolysis over both natural olivine and NiALO catalyst displayed a notably reduction of NH_3 emissions. These results are is in accordance with the statement that iron and nickel catalyzes the decomposition of NH_3 into N_2 and H_2 [75,76]. Nickel-based catalysts were found available for NH_3 abatement in produced coal syngas at high temperature and pressures [77,78]. So, decreasing NH_3 evolution by decomposition will allowed to lower the NO_x emissions in subsequently combustion/gasification stage.

The temperature-concentration curves of NO_x, specifically NO_2 and NO, respectively, under non catalytic and catalytic coal pyrolysis is shown in Figs. 6C and 6(D). The formation of NO_2 and NO under inert atmosphere were already observed in coals pyrolysis [79]. It is known that nitrogen in coal is basically found as nitrogen oxides, quaternary (N–Q), pyridinic (N-6) and pyrrolic (N-5) groups that are converted to gaseous compounds like HCN and NH_3 under pyrolysis conditions [80]. The NO_2 evolution from coal alone appeared between 300 and 700 °C through two overlapping peaks, which were quite diminished in catalytic coal pyrolysis (Fig. 6C). The NO emission from coal pyrolysis in the presence of additives has been observed at very low temperatures, unlike coal pyrolysis alone (Fig. 6D). The formation of NO during coal pyrolysis come from the combination of nitrogen and oxygen functional group [81], which can be catalysed by both iron and nickel metals.

3.3. TG/DTG/DSC analysis

In Fig. 7(a) and (b) are showed the TG/DTG curves simulating the whole N_2 -pyrolysis process of raw coal, mixture of coal/olivine, and mixture of coal/NiALO catalyst from room temperature to 900 °C at

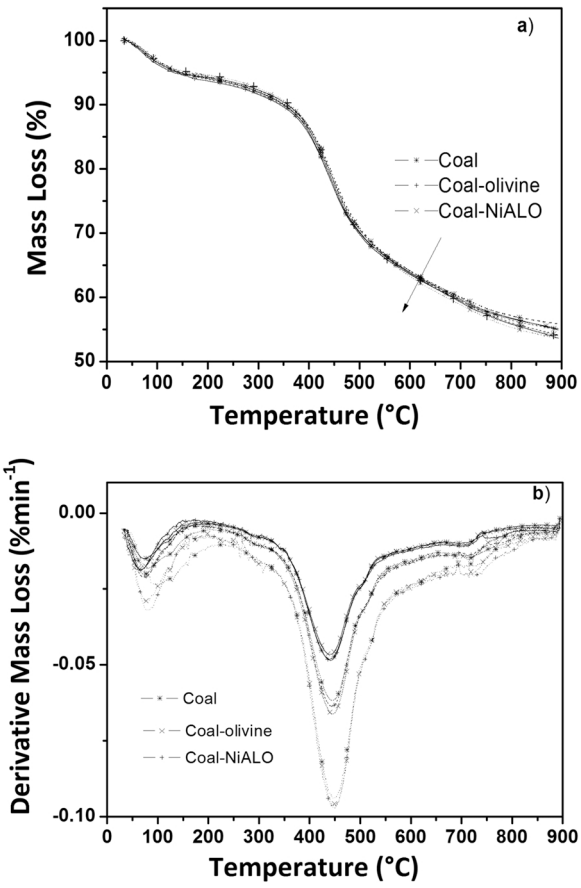

Fig. 7. TG (a) and DTG (b) curves of N_2-pyrolysis of Sulcis coal and mixture of Sulcis coal with olivine and NiALO catalyst at 15(—), 20(- -), and 30(··) °Cmin^{-1} heating rate.

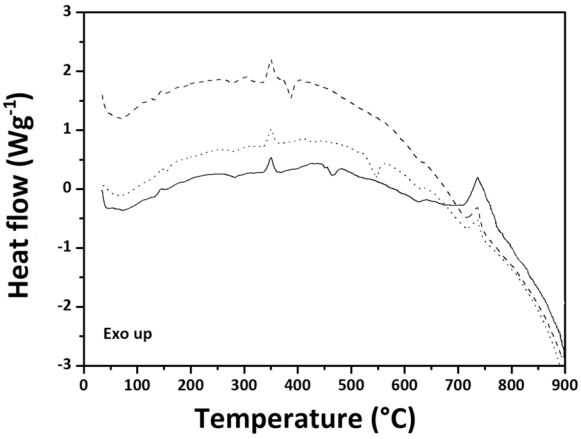

Fig. 8. DSC curves of N_2-pyrolysis of Sulcis coal (-) and mixture of Sulcis coal with olivine (- -) and NiALO catalyst (··) at 15°Cmin^{-1} heating rate.

different heating rates (β = 15, 20, and 30 °C•min^{-1}). The corresponding heat flows (DSC curves) at β = 15 °C•min^{-1} were reported in Fig. 8. The TG curves of all the samples presented the same profiles and the curves were slightly shifted at higher temperature with increasing of heating rate. Thermal decomposition of raw coal with additives yielded larger mass losses, typically around 3% of the starting raw sample mass. As previously reported in [35], the three principal regions of mass losses recognized on the TG curves were simplistically ascribed to: i) dehydration, ii) devolatilization of more labile/stable volatiles, and iii) char

formation. Meanwhile, four maximum peaks on the DTG curves were distinctly observed at about 60, 300, 450, and 700 °C. The corresponding DSC curves at β = 15 °C•min^{-1} displayed both endothermic/exothermic effects. Previously DSC studies on coal pyrolysis with different rank from anthracite to lignite showed that the net heat events occurring during coal pyrolysis were mainly endothermic in nature [82]. In the present study, the first large endothermic peak between room temperature to 200 °C was due to removal of moisture, followed by a second very small endothermic peak at about 290 °C. It was reported that in the temperature region 200–350 °C coals start to lose small amounts of pyrolysis water from decomposing phenolic structures, and oxides of carbon from carboxylic and carbonyl groups, which are endothermic events [83]. The exothermic event at temperature above 300 °C was associated with the primary carbonization process and development of plastic phase prior to char formation [83,84]. Meanwhile for coal/NiALO mixture an extra endothermic peak around 400 °C appeared just after the exothermic heat of primary pyrolysis, which would be due to catalyzed volatilization of organic matter. An exothermic event was often reported at 430 °C for high volatile sub bituminous coal [84]. For the coal/olivine mixture an extra sharp endothermic peak at 550 °C was observed, which may be attributable to the transformation of pyrite present in Sulcis coal to pyrrhotite [85]. A further small endothermic peak at about 630 °C might be ascribed to gasification of char with CO evolution, which is endothermic in nature [82]. The strong exothermic peak near 750 °C was due to condensation/polymerization of aromatic structures in char to yield H_2 [86].

3.3.1. Kinetic analysis

The kinetic parameters were derived from non-isothermal TG data using an isoconversional model-free method to derive the activation energy (E_a) and pre-exponential factor of non-catalytic and catalytic coal pyrolysis as recommended by the ICTAC Kinetic Committee [87]. The isoconversional principle affirms that the reaction rate at a fixed extent of conversion α depends only on temperature. Thus, the E_a on conversion (α) dependence is evaluated by using multiple temperature programs under different temperature heating rates [88]. The rate of kinetic process can be defined by the Arrhenius type equation under linear heating rate (β = dT/dt) as follows [87]:

$$\frac{d\alpha}{dt} = \beta\frac{d\alpha}{dT} = Ae^{-E/RT}f(\alpha) \tag{3}$$

where $\frac{d\alpha}{dt}$ or $\beta\frac{d\alpha}{dT}$ is the rate of process, T(K) is the absolute temperature, E (kJ mol^{-1}) is the activation energy, A (min^{-1}) is the pre-exponential factor, R (8.3143 kJ K^{-1} mol^{-1}) is the universal gas constant, β (K min^{-1}) is the heating rate, f(α) is a function of the reaction mechanism and α is the thermochemical conversion expressed in terms of mass change of solids as follows:

$$\alpha = \frac{m_0 - m_t}{m_0 - m_f} \tag{4}$$

where m_0, is the initial sample mass, m_t is the sample mass at time t, and m_f is the sample mass at the end of each non-isothermal TG run. The m_0 was taken at temperature around 350 °C in order to eliminate the mass loss due to absorbed water and more labile compounds volatilization. The integration of Eq. (1) after separation of variables lead to the following expression:

$$g(\alpha) = \int_0^{\alpha}\frac{d\alpha}{f(\alpha)} = \int_{T_0}^{T} e^{-E/RT}dT \cong \frac{AE}{\beta R}p(x) \tag{5}$$

where $g(\alpha)$ is the integral form of $f(\alpha)$ and $p(x)$ of temperature integral. However, $p(x)$ does not allow an analytical solution but several approximations can be found in the literature [89–91]. According to the most temperature integral approximations of the Starink method [92,93], a linear equation of the general form can be written below [87]:

$$Ln\left(\frac{\beta_i}{T_{\alpha,i}^{1.92}}\right) = const - 1.0008\frac{E_\alpha}{RT_\alpha} \tag{6}$$

For a given conversion (α) value the activation energy can be calculated from the slope of the $Ln\left(\frac{\beta_i}{T_{\alpha,i}^{1.92}}\right)$ – 1/T curves obtained at different heating rates. In Fig. 9 are depicted the isoconvertional lines of coal pyrolysis with and without additives, which presented correlation coefficients R^2 better than 0.99. It is worth to note that the fit to a straight line was only possible in a narrow range of conversion, namely 0–0.3, 0–0.5, and 0–0.5 for coal alone, coal-olivine, and coal-NiALO, respectively, because little o no correlation of the obtained results was existing for high conversion values. In Fig. 10 the variation of activation energies and the pre-exponential factors as a function of conversion (α) was compared for coal pyrolysis with and without additives. All the samples showed similar behavior. At low conversion values the initial activation energy values were low due to loss of volatile substances with the breaking of weak bonds in coal. With the progress of conversion the activation energy values increased and then remained almost constant within a certain conversion range, which was wider for coal-additive mixtures.These results indicate that a single-step reaction process was operative, with the evident beneficial effect of the additives on coal pyrolysis. As expected, for higher conversion values a sharply increasing of activation energy occurred, probably associated with the initial process of char formation [53], which is accompanied by a complex relationship between E and α due to multi-step reactions. The average value of activation energy calculated by isoconversional method for coal pyrolysis alone was 179 kJ mol^{-1} in accordance with the value found at higher heating rates [35,94]. The average E_a values for coal-olivine pyrolysis and coal-NiALO pyrolysis were 147 and 143 kJ mol^{-1}, respectively. The lowering of activation energy by 40% with addition of olivine and Ni-based catalyst to raw coal was in accordance with reported investigation that the presence of catalyst diminishes the amount of energy required to degrade the organic matter of coal during pyrolysis [95]. The pre-exponential factors were also decreased.

3.3.2. Kinetic compensation effect

The Arrhenius parameters of energy of activation and pre-exponential factor could have strong correlation each other such that the increase of one leads to a compensatory effect on the other, the so-called kinetic compensation effect [96]. Specifically, with the variation of the heating rate, a linear relationship between the logarithm of the pre-exponential factor (lnA) and the activation energy exists according to the following equation:

$$\mathrm{LnA} = \mathrm{a} + \mathrm{bE} \tag{7}$$

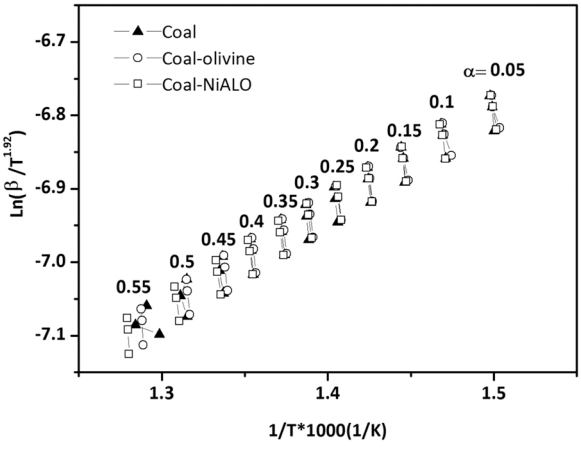

Fig. 9. Isoconversional lines at different conversion α values for non-catalytic and catalytic coal pyrolysis.

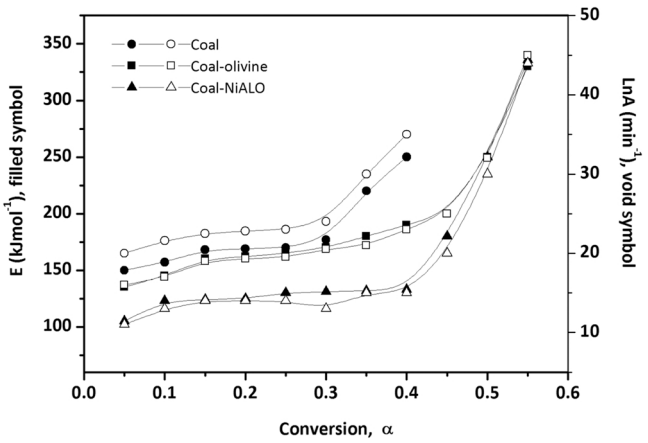

Fig. 10. Activation energy (E) and pre-exponential factor A dependence on α for non-catalytic and catalytic coal pyrolysis non-isothermal data evaluated by isoconversional method.

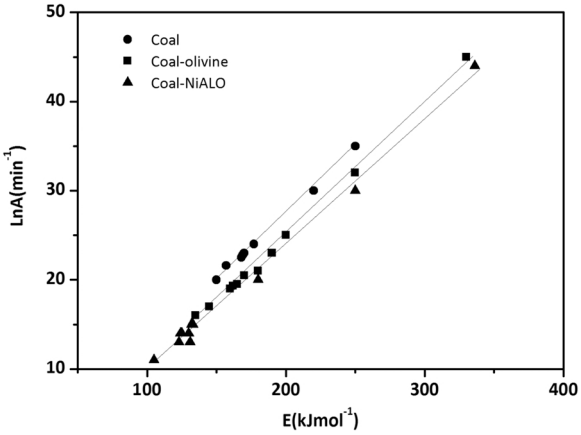

Fig. 11. Kinetic compensation effect for non-catalytic and catalytic coal pyrolysis.

where the constants a and b were referred to compensation parameters and founded by linear regression. Fig. 11 shows the linear correlation between E and LnA according to the Eq. (7) with R^2 better than 0.99 at different conversion values. The occurrence of kinetic compensation effect has proven the kinetic model adopted well represents the coal pyrolysis with and without catalyst. The average pre-exponential factor was calculated from Eq. (7) using the average energy of activation found by the model-free method. It was found values of pre-exponential factor $A_0 = 5.3 \times 10^8$, 1.8×10^6, and 5.7×10^5 min^{-1} for raw coal, mixture of coal/olivine and coal/NiALO, respectively.

4. Conclusions

Natural olivine and home-made 15 wt%Ni/γ-Al_2O_3 catalyst showed beneficial catalytic effect on N_2-pyrolysis of Sulcis low-rank coal at low temperature by enhancing the pyrolysis gas yield. Nickel-based catalyst mainly enhanced the content of CO_2, CO, and H_2 in gas effluent, which is advisable for syngas production. Conversely, little impact was seen in the gaseous production of CH_4 and C_2-C_6 hydrocarbons, exception made for ethene yield. Olivine had good impact in sulphur removal through enhanced SO_2 emission during N_2-pyrolysis, as well N-containing compounds (NH_3, NO_x) were also modified in catalytic pyrolysis. Kinetic studies of catalytic pyrolysis testify that in the conversion range 0.05–0.5 a single-step mechanism of thermal degradation is operative and the presence of additives was able to decrease the activation energy of coal pyrolysis.

Declaration of Competing Interest

The author declares that she has no known competing financial interest or personal relationships that could have appeared to influence the work reported in this paper.

Data Availability

The authors do not have permission to share data.

References

[1] F. Mushtaq, R. Mat, F.N. Ani, A review on microwave assisted pyrolysis of coal and biomass for fuel production, Renew. Sustain. Energy Rev. 39 (2014) 555–574, https://doi.org/10.1016/j.rser.2014.07.073.
[2] K.H. Van Heek, W. Hodek, Structure and pyrolysis behaviour of different coals and relevant model substances, Fuel 73 (1994) 886–896, https://doi.org/10.1016/0016-2361(94)90283-6.
[3] P.R. Solomon, T.H. Fletcher, R.J. Pugmire, Progress in coal pyrolysis, Fuel 72 (1993) 587–597, https://doi.org/10.1016/0016-2361(93)90570-R.
[4] A. Arenillas, F. Rubiera, C. Pevida, J.J. Pis, A comparison of different methods for predicting coal devolatilisation kinetics, J. Anal. Appl. Pyrolysis 58 (2001) 685–701, https://doi.org/10.1016/S0165-2370(00)00183-2.
[5] B. Dou, J. Gao, X. Sha, S.W. Baek, Catalytic cracking of tar component from high-temperature fuel gas, Appl. Therm. Eng. 23 (2003) 2229–2239, https://doi.org/10.1016/S1359-4311(03)00185-6.
[6] A. Tomita, O. Yasuo, T. Yasukatsu, Low temperature gasification of brown coals catalysed by nickel, Fuel 62 (1983) 150–154, https://doi.org/10.1016/0016-2361(83)90187-4.
[7] Q. Liu, H. Hu, Q. Zhou, S. Zhu, G. Chen, Effect of inorganic matter on reactivity and kinetics of coal pyrolysis, Fuel 83 (2004) 713–718, https://doi.org/10.1016/j.fuel.2003.08.017.
[8] R. Cypres, C. Soudan-Moinet, Pyrolysis of coal and iron oxides mixtures. 1. Influence of iron oxides on the pyrolysis of coal, Fuel 59 (1980) 48–54, https://doi.org/10.1016/0016-2361(80)90010-1.
[9] S. Lin, M. Harada, Y. Suzuki, H. Hatano, Comparison of pyrolysis products between coal, coal/CaO, and coal/$Ca(OH)_2$ materials, Energy Fuels 17 (2003) 602–607, https://doi.org/10.1021/ef020204w.
[10] L. Devi, M. Craje, P. Thüne, K.J. Ptasinski, F.J. Janssen, Olivine as tar removal catalyst for biomass gasifiers: catalyst characterization, Appl. Catal. A: Gen. 294 (2005) 68–79, https://doi.org/10.1016/j.apcata.2005.07.044.
[11] M.W. Islam, A review of dolomite catalyst for biomass gasification tar removal, Fuel 267 (2020), 117095, https://doi.org/10.1016/j.fuel.2020.117095.
[12] X. Ma, X. Zhao, J. Gu, J. Shi, Co-gasification of coal and biomass blends using dolomite and olivine as catalysts, Renew. Energy 132 (2019) 509–514, https://doi.org/10.1016/j.renene.2018.07.077.
[13] J.N. Kuhn, Z. Zhao, L.G. Felix, R.B. Slimane, C.W. Choi, U.S. Ozkan, Olivine catalysts for methane-and tar-steam reforming, Appl. Catal. B: Environ. 81 (2008) 14–26, https://doi.org/10.1016/j.apcatb.2007.11.040.
[14] S. Rapagnà, N. Jand, A. Kiennemann, P.U. Foscolo, Steam-gasification of biomass in a fluidised-bed of olivine particles, Biomass Bioenergy 19 (2000) 187–197, https://doi.org/10.1016/S0961-9534(00)00031-3.
[15] L. Devi, K.J. Ptasinski, F.J. Janssen, S.V. van Paasen, P.C. Bergman, J.H. Kiel, Catalytic decomposition of biomass tars: use of dolomite and untreated olivine, Renew. Energy 30 (2005) 565–587, https://doi.org/10.1016/j.renene.2004.07.014.
[16] T. Nordgreen, T. Liliedahl, K. Sjöström, Metallic iron as a tar breakdown catalyst related to atmospheric, fluidised bed gasification of biomass, Fuel 85 (2006) 689–694, https://doi.org/10.1016/j.fuel.2005.08.026.
[17] H. Matsuhashi, H. Nakamura, K. Arata, R. Yoshida, Y. Maekawa, Catalytic activities of metal oxides containing iron for hydrocracking coal model compounds and Taiheiyo coal, Fuel 76 (1997) 913–918, https://doi.org/10.1016/S0016-2361(97)00089-6.
[18] Y. Nishiyama, Catalytic behaviour of iron and nickel in coal gasification, Fuel 65 (1986) 1404–1409, https://doi.org/10.1016/0016-2361(86)90114-6.
[19] T. Kimura, T. Miyazawa, J. Nishikawa, S. Kado, K. Okumura, T. Miyao, S. Naito, K. Kunimori, K. Tomishige, Development of Ni catalysts for tar removal by steam gasification of biomass, Appl. Catal. B Environ. 68 (2006) 160–170, https://doi.org/10.1016/j.apcatb.2006.08.007.
[20] M. Wang, L. Jin, Y. Li, J. Lv, B. Wei, H. Hu, In-situ catalytic upgrading of coal pyrolysis tar coupled with CO_2 reforming of methane over Ni-based catalysts, Fuel Process. Technol. 177 (2018) 119–128, https://doi.org/10.1016/j.fuproc.2018.04.022.
[21] Y. Li, M.N. Amin, X. Lu, C. Li, F. Ren, S. Zhang, Pyrolysis and catalytic upgrading of low-rank coal using a NiO/MgO-Al_2O_3 catalyst, Chem. Eng. Sci. 155 (2016) 194–200, https://doi.org/10.1016/j.ces.2016.08.003.
[22] J. Han, X. Liu, J. Yue, B. Xi, S. Gao, G. Xu, Catalytic upgrading of in situ coal pyrolysis tar over Ni-char catalyst with different additives, Energy Fuels 28 (2014) 4934–4941, https://doi.org/10.1021/ef500927d.

[23] M.N. Amin, Y. Li, R. Razzaq, X. Lu, C. Li, S. Zhang, Pyrolysis of low rank coal by nickel based zeolite catalysts in the two-staged bed reactor, J. Anal. Appl. Pyrolysis 118 (118) (2016) 54–62, https://doi.org/10.1016/j.jaap.2015.11.019.
[24] A. Arregi, G. Lopez, M. Amutio, I. Barbarias, L. Santamaria, J. Bilbao, M. Olazar, Kinetic study of the catalytic reforming of biomass pyrolysis volatiles over a commercial Ni/Al_2O_3 catalyst, Int. J. Hydrog. Energy 43 (2018) 12023–12033, https://doi.org/10.1016/j.ijhydene.2018.05.032.
[25] S. Cao, D. Wang, M. Wang, J. Zhu, L. Jin, Y. Li, H. Hu, In-situ upgrading of coal pyrolysis tar with steam catalytic cracking over Ni/Al_2O_3 catalysts, Chem. Sel. 6 (2020) 4905–4912, https://doi.org/10.1016/j.ijhydene.2018.05.032.
[26] L.B. Råberg, M.B. Jensen, U. Olsbye, C. Daniel, S. Haag, C. Mirodatos, A.O. Sjåstad, Propane dry reforming to synthesis gas over Ni-based catalysts: influence of support and operating parameters on catalyst activity and stability, J. Catal. 249 (2007) 250–260, https://doi.org/10.1016/j.jcat.2007.04.004.
[27] W.C. Xu, A. Tomita, Effect of metal oxides on the secondary reactions of volatiles from coal, Fuel 68 (1989) 673–676, https://doi.org/10.1016/0016-2361(89)90173-7.
[28] J. Ashok, Y. Kathiraser, M.L. Ang, S. Kawi, Bi-functional hydrotalcite-derived NiO–CaO–Al_2O_3 catalysts for steam reforming of biomass and/or tar model compound at low steam-to-carbon conditions, Appl. Catal. B Environ. 172 (2015) 116–128, https://doi.org/10.1016/j.apcatb.2015.02.017.
[29] Y. Wang, Y. Li, G. Wang, J. Zhu, H. Yang, L. Jin, S. Hu, H. Hu, In-situ catalytic upgrading of coal pyrolysis volatiles over red mud-supported nickel catalysts, Fuel 324 (2022), 124742, https://doi.org/10.1016/j.fuel.2022.124742.
[30] P. Zhu, Z. Yu, J. Zhang, B. Dai, J. Zhang, P. Liang, Z. Lei, Catalytic pyrolysis of bituminous coal under pyrolysis gas over a Ni/MgO catalyst, Chem. Eng. Technol. 40 (2017) 1605–1610, https://doi.org/10.1002/ceat.201700163.
[31] T.L. Liu, J.P. Cao, X.Y. Zhao, J.X. Wang, X.Y. Ren, X. Fan, Y.P. Zhao, X.Y. Wei, In situ upgrading of Shengli lignite pyrolysis vapors over metal-loaded HZSM-5 catalyst, Fuel Process. Technol. 160 (2017) 19–26, https://doi.org/10.1016/j.fuproc.2017.02.012.
[32] Z. Shi, L. Jin, Y. Zhou, H. Li, Y. Li, H. Hu, In-situ analysis of catalytic pyrolysis of Baiyinhua coal with pyrolysis time-of-flight mass spectrometry, Fuel 227 (2018) 386–393, https://doi.org/10.1016/j.fuel.2018.04.109.
[33] X.Y. Ren, J.P. Cao, X.Y. Zhao, Z. Yang, T.L. Liu, X. Fan, X.Y. Wei, Catalytic upgrading of pyrolysis vapors from lignite over mono/bimetal-loaded mesoporous HZSM-5, Fuel 15 (2018) 33–40, https://doi.org/10.1016/j.fuel.2018.01.017.
[34] S. Scaccia, A. Calabrò, R. Mecozzi, Investigation of the evolved gases from Sulcis coal during pyrolysis under N_2 and H_2 atmospheres, J. Anal. Appl. Pyrolysis 98 (2012) 45–50, https://doi.org/10.1016/j.jaap.2012.05.001.
[35] S. Scaccia, TG–FTIR and kinetics of devolatilization of Sulcis coal, J. Anal. Appl. Pyrolysis 104 (2013) 95–102, https://doi.org/10.1016/j.jaap.2013.09.002.
[36] A. Pineau, N. Kanari, I. Gaballah, Kinetics of reduction of iron oxides by H_2: Part I: Low temperature reduction of hematite, Thermochim. Acta 447 (2006) 89–100, https://doi.org/10.1016/j.tca.2005.10.004.
[37] M.H. Jeong, D.H. Lee, J.W. Bae, Reduction and oxidation kinetics of different phases of iron oxides, Int. J. Hydrog. Energy 40 (2015) 2613–2620, https://doi.org/10.1016/j.ijhydene.2014.12.099.
[38] S. Scaccia, L. Della Seta, D. Mirabile Gattia, G. Vanga, Catalytic performance of Ni/CaO-$Ca_{12}Al_{14}O_{33}$ catalyst in the green synthesis gas production via CO_2 reforming of CH_4, J. CO_2 Util. 45 (2021) 01447, https://doi.org/10.1016/j.jcou.2021.101447.
[39] ⟨https://www.gasmet.com/products/software/⟩.
[40] P.R. Solomon, M.A. Serio, E.M. Suuberg, Coal pyrolysis: experiments, kinetic rates and mechanisms, Prog. Energy Combust. Sci. 18 (1992) 133–220, https://doi.org/10.1016/0360-1285(92)90021-R.
[41] X. Qi, D. Wang, H. Xin, G. Qi, In situ FTIR study of real-time changes of active groups during oxygen-free reaction of coal, Energy Fuels 27 (2013) 3130–3136, https://doi.org/10.1021/ef400534f.
[42] A. Arenillas, F. Rubiera, J.J. Pis, Simultaneous thermogravimetric–mass spectrometric study on the pyrolysis behaviour of different rank coals, J. Anal. Appl. Pyrolysis 50 (1999) 31–46, https://doi.org/10.1016/S0165-2370(99)00024-8.
[43] Q. Song, H. Zhao, S. Chang, L. Yang, F. Zou, X. Shu, P. Zhang, Study on the catalytic pyrolysis of coal volatiles over hematite for the production of light tar, J. Anal. Appl. Pyrolysis 151 (2020), 104927, https://doi.org/10.1016/j.jaap.2020.104927.
[44] H. Zhao, Y. Li, Q. Song, J. Lv, Y. Shu, X. Liang, X. Shu, Effects of iron ores on the pyrolysis characteristics of a low-rank bituminous coal, Energy Fuels 30 (2016) 3831–3839, https://doi.org/10.1021/acs.energyfuels.6b00061.
[45] F. Guo, X. Jia, S. Liang, N. Zhou, P. Chen, R. Ruan, Development of biochar-based nanocatalysts for tar cracking/reforming during biomass pyrolysis and gasification, Bioresour. Technol. 298 (2020) 12263, https://doi.org/10.1016/j.biortech.2019.122263.
[46] J. Liu, X. Jiang, J. Shen, H. Zhang, Pyrolysis of superfine pulverized coal. Part 2. Mechanisms of carbon monoxide formation, Energy Convers. Manag. 87 (2014) 1039–1049, https://doi.org/10.1016/j.enconman.2014.07.055.
[47] C. Wu, Z. Wang, J. Huang, P.T. Williams, Pyrolysis/gasification of cellulose, hemicellulose and lignin for hydrogen production in the presence of various nickel-based catalysts, Fuel 106 (2013) 697–706, https://doi.org/10.1016/j.fuel.2012.10.064.
[48] S. Porada, The influence of elevated pressure on the kinetics of evolution of selected gaseous products during coal pyrolysis, Fuel 83 (2004) 1071–1078, https://doi.org/10.1016/j.fuel.2003.11.004.
[49] S. Porada, The reactions of formation of selected gas products during coal pyrolysis, Fuel 83 (2004) 1191–1196, https://doi.org/10.1016/j.fuel.2003.11.007.
[50] J.H. Campbell, Pyrolysis of subbituminous coal in relation to in-situ coal gasification, Fuel 57 (1978) 217–224, https://doi.org/10.1016/0016-2361(78)90119-9.
[51] L. Shi, Q. Liu, B. Zhou, X. Guo, Z. Li, X. Cheng, R. Yang, Z. Liu, Interpretation of methane and hydrogen evolution in coal pyrolysis from the bond cleavage perspective, Energy Fuels 31 (2017) 429–437, https://doi.org/10.1021/acs.energyfuels.6b02482.
[52] X. Li, B.M. Krooss, P. Weniger, R. Littke, Liberation of molecular hydrogen (H_2) and methane (CH_4) during non-isothermal pyrolysis of shales and coals: Systematics and quantification, Int. J. Coal Geol. 137 (2015) 152–164, https://doi.org/10.1016/j.coal.2014.11.011.
[53] M.A. Serio, D.G. Hamblen, J.R. Markham, P.R. Solomon, Kinetics of volatile product evolution in coal pyrolysis: experiment and theory, Energy Fuels 1 (1987) 138–152, https://doi.org/10.1021/ef00002a002.
[54] B. Bayarsaikhan, N. Sonoyama, S. Hosokai, T. Shimada, J. Hayashi, C.Z. Li, T. Chiba, Inhibition of steam gasification of char by volatiles in a fluidised bed under continous feeding of a brown coal, Fuel 85 (2006) 340–349, https://doi.org/10.1016/j.fuel.2005.06.001.
[55] Y. Huang, X. Yin, C. Wu, C. Wang, J. Xie, Z. Zhou, L. Ma, H. Li, Effects of metal catalysts on CO_2 gasification reactivity of biomass char, Biotechnol. Adv. 27 (2009) 568–572, https://doi.org/10.1016/j.biotechadv.2009.04.013.
[56] Y. Nishiyama, Catalytic behaviour of iron and nickel in coal gasification, Fuel 65 (1983) 1404–1409, https://doi.org/10.1016/0016-2361(86)90114-6.
[57] J. Liu, X. Jiang, J. Shen, H. Zhang, Pyrolysis of superfine pulverized coal. Part 1. Mechanisms of methane formation, Energy Convers. Manag. 87 (2014) 1027–1038, https://doi.org/10.1016/j.enconman.2014.07.053.
[58] D. Alsaab, M. Elie, A. Izart, R.F. Sachsenhofer, V.A. Privalov, I. Suarez-Ruiz, L. Martinez, Comparison of hydrocarbons gases (C_1-C_5) production from Carboniferous Donets (Ukraine) and Cretaceous Sabinas (Mexico) coals, Int. J. Coal Geol. 74 (2008) 154–162, https://doi.org/10.1016/j.coal.2007.11.006.
[59] P.F. Nelson, I.W. Smith, R.J. Tyler, J.C. Mackie, Pyrolysis of coal at high temperatures, Energy Fuels 2 (1988) 391–400, https://doi.org/10.1021/ef00010a004.
[60] H. Song, G. Liu, J. Zhang, J. Wu, Pyrolysis characteristics and kinetics of low rank coals by TG-FTIR method, Fuel Process. Technol. 156 (2017) 454–460, https://doi.org/10.1016/j.fuproc.2016.10.008.
[61] K.R. Squire, P.R. Solomon, R.M. Carangelo, M.B. DiTaranto, Tar evolution from coal and model polymers 2, Eff. Aromat. ring sizes donatable Hydrog., Fuel 65 (1988) 833–843, https://doi.org/10.1016/0016-2361(86)90078-5.
[62] P.A. Simell, J.S. Bredenberg, Catalytic purification of tarry fuel gas, Fuel 69 (1990) 1219–1225, https://doi.org/10.1016/0016-2361(90)90280-4.
[63] Q. Song, H. Zhao, Q. Ma, L. Yang, L. Ma, Y. Wu, P. Zhang, Catalytic upgrading of coal volatiles with Fe_2O_3 and hematite by TG-FTIR and Py-GC/MS, Fuel 313 (2022), 122667, https://doi.org/10.1016/j.fuel.2021.122667.
[64] C. Amen-Chen, H. Pakdel, C. Roy, Production of monomeric phenols by thermochemical conversion of biomass: a review, Bioresour. Technol. 79 (2001) 277–299, https://doi.org/10.1016/S0960-8524(00)00180-2.
[65] S. Wang, K. Wang, Q. Liu, Y. Gu, Z. Luo, K. Cen, T. Fransson, Comparison of the pyrolysis behavior of lignins from different tree species, Biotechnol. Adv. 27 (2009) 562–567, https://doi.org/10.1016/j.biotechadv.2009.04.010.
[66] M. Cortazar, L. Santamaria, G. Lopez, J. Alvarez, M. Amutio, J. Bilbao, M. Olazar, Fe/olivine as primary catalyst in the biomass steam gasification in a fountain confined spouted bed reactor, J. Ind. Eng. Chem. 99 (2021) 364–379, https://doi.org/10.1016/j.jiec.2021.04.046.
[67] S. Yani, D.K. Zhang, Transformation of organic and inorganic sulphur in a lignite during pyrolysis: influence of inherent and added inorganic matter, Proc. Combust. Inst. 32 (2009) 2083–2089, https://doi.org/10.1016/j.proci.2008.06.189.
[68] A. Attar, Chemistry, thermodynamics and kinetics of reactions of sulphur in coal-gas reactions: a review, Fuel 57 (1978) 201–212, https://doi.org/10.1016/0016-2361(78)90117-5.
[69] J. Yan, J. Yang, Z. Liu, SH radical: the key intermediate in sulfur transformation during thermal processing of coal, Environ. Sci. Technol. 39 (2005) 5043–5051, https://doi.org/10.1021/es048398c.
[70] S. Furfari, R. Cyprès, Hydropyrolysis of a high-sulphur-high-calcite Italian Sulcis coal. 2. Importance of the mineral matter on the sulphur behaviour, Fuel 61 (1982) 453–459, https://doi.org/10.1016/0016-2361(82)90071-0.
[71] H. Cheng, Q. Liu, M. Huang, S. Zhang, R.L. Frost, Application of TG-FTIR to study SO_2 evolved during the thermal decomposition of coal-derived pyrite, Thermochim. Acta 555 (2013) 1–6, https://doi.org/10.1016/j.tca.2012.12.025.
[72] Y. Gu, J. Yperman, J. Vandewijngaardden, G. Reggers, R. Carleer, Organic and inorganic sulphur compounds releases from high-pyrite coal pyrolysis in H_2, N_2 and CO_2: test case Chinese LZ coal, Fuel 202 (2017) 494–502, https://doi.org/10.1016/j.fuel.2017.04.068.
[73] F.J. Tian, J. Yu, L.J. McKenzie, J. Hayashi, C.Z. Li, Conversion of fuel-N into HCN and NH_3 during the pyrolysis and gasification in steam: a comparative study of coal and biomass, Energy Fuels 21 (2007) 517–521, https://doi.org/10.1021/ef060415r.
[74] C.Z. Li, L.L. Tan, Formation of NO_x and SO_x precursors during the pyrolysis of coal and biomass. Part III. Further discussion on the formation of HCN and NH_3 during pyrolysis, Fuel 79 (2000) 1899–1906, https://doi.org/10.1016/S0016-2361(00)00008-9.
[75] H. Mori, K. Asami, Y. Ohtsuka, Role of iron catalyst in fate of fuel nitrogen during coal pyrolysis, Energy&Fuels 10 (1996) 1022–1027, https://doi.org/10.1021/ef960035d.
[76] M. Feyen, C. Weidenthaler, R. Güttel, K. Schlichte, U. Holle, A.H. Lu, F. Schüth, High-temperature stable, iron-based core–shell catalysts for ammonia

decomposition, Chem. A Eur. J. 17 (2011) 598–605, https://doi.org/10.1002/chem.201001827.
[77] J. Leppälahti, P. Simell, E. Kurkela, Catalytic conversion of nitrogen compounds in gasification gas, Fuel Process. Technol. 29 (1991) 43–56, https://doi.org/10.1016/0378-3820(91)90016-6.
[78] S. Kambara, T. Takarada, Y. Yamamoto, K. Kato, Relation between functional forms of coal nitrogen and formation of nitrogen oxide (NO_x) precursors during rapid pyrolysis, Energy Fuels 7 (1993) 1013–1020.
[79] A. Arenillas, C. Pevida, F. Rubiera, R. Garcia, J.J. Pis, Characterization of model compounds and a synthetic coal by TG/MS/FTIR to represent the pyrolysis behavior coal, J. Anal. Appl. Pyrolysis 71 (2004) 747–763, https://doi.org/10.1016/j.jaap.2003.10.005.
[80] J. Liu, X. Jiang, J. Shen, H. Zhang, Pyrolysis of superfine pulverized coal. Part 3. Mechanisms of nitrogen-containing species formation, Energy Convers. Manag. 94 (2015) 130–138, https://doi.org/10.1016/j.enconman.2014.12.096.
[81] X. Xiong, S. Yu, D. Qin, H. Tan, X. Lu, Evolution behaviors of the nitrogen-containing species and SO_2 from coal fast pyrolysis, J. Energy Inst. 105 (2022) 133–140, https://doi.org/10.1016/j.joei.2022.08.009.
[82] P.J.J. Tromp, F. Kapteijn, J.A. Moulijn, Characterization of coal pyrolysis by means of differential scanning calorimetry. 1. Quantitative heat effects in an inert atmosphere, Fuel Process. Technol. 15 (1987) 45–57, https://doi.org/10.1016/0378-3820(87)90033-6.
[83] J.P. Elder, M.B. Harris, Thermogravimetry and differential scanning calorimetry of Kentucky bituminous coals, Fuel 63 (1984) 262–267, https://doi.org/10.1016/0016-2361(84)90048-6.
[84] P.I. Gold, Thermal analysis of exothermic processes in coal pyrolysis, Thermochim. Acta 42 (1980) 135–152, https://doi.org/10.1016/0040-6031(80)87098-5.
[85] S.K. Bhargava, A. Garg, N.D. Subasinghe, In situ high-temperature phase transformation studies on pyrite, Fuel (2009) 988–993, https://doi.org/10.1016/j.fuel.2008.12.005.
[86] P.J.J. Tromp, F. Kapteijn, J.A. Moulijn, Characterization of coal pyrolysis by means of differential scanning calorimetry. 1. Quantitative heat effects in an inert atmosphere, Fuel Process. Technol. 15 (1987) 45–57, https://doi.org/10.1016/0378-3820(87)90033-6.
[87] S. Vyazovkin, A.K. Burnham, J.M. Criado, L.A. Pérez-Maqueda, C. Popescu, N. Sbirrazzuoli, ICTAC Kinetics Committee recommendations for performing kinetic computations on thermal analysis data, Thermochim. Acta 520 (2011) 1–19, https://doi.org/10.1016/j.tca.2011.03.034.
[88] S. Vyazovkin, A.K. Burnham, L. Favergeon, N. Koga, E. Moukhina, L.A. Pérez-Maqueda, N. Sbirrazzuoli, ICTAC Kinetics Committee recommendations for analysis of multi-step kinetics, Thermochim. Acta 689 (2020), 178597, https://doi.org/10.1016/j.tca.2020.178597.
[89] J.H. Flynn, L.A. Wall, A quick, direct method for the determination of activation energy from thermogravimetric data, Polym. Lett. 4 (1966) 323–328, https://doi.org/10.1002/pol.1966.110040504.
[90] H.L. Friedman, Kinetics of thermal degradation of char-forming plastics from thermogravimetry. Application to a phenolic plastic, J. Polym. Sci. Part C. 6 (1964) 183–195, https://doi.org/10.1002/polc.5070060121.
[91] C.D. Doyle, Series approximations to the equations of thermogravimetric data, Nature 207 (1965) 290–291, https://doi.org/10.1038/207290a0.
[92] M.J. Starink, The determination of activation energy from linear heating rate experiments: a comparison of the accuracy of isoconversion methods, Thermochim. Acta 404 (2003) 163–176, https://doi.org/10.1016/S0040-6031(03)00144-8.
[93] M.J. Starink, Activation energy determination for linear heating experiments: deviations due to neglecting the low temperature end of the temperature integral, J. Mater. Sci. 42 (2007), 483489, https://doi.org/10.1007/s10853-006-1067-7.
[94] H. Chi, H. Li, S. Hu, A.A. Shagali, H. Qing, J. Xu, J. Xu, L. Jiang, Y. Wang, S. Su, J. Xiang, Pyrolysis characteristics and kinetic study of coal in a novel concentrating photothermal thermogravimetric analyzer: effect of heating rate, Fuel 322 (2022), 124218, https://doi.org/10.1016/j.fuel.2022.124218.
[95] Y. Fu, Y.H. Guo, K.X. Zhang, Effect of three different catalysts (KCl, CaO, and Fe_2O_3) on the reactivity and mechanism of low-rank coal pyrolysis, Energy Fuels 30 (2016) 2428–2433, https://doi.org/10.1021/acs.energyfuels.5b02720.
[96] M.E. Brown, A.K. Galwey, The significance of “compensation effects” appearing in data published in “computational aspects of kinetic analysis”: ICTAC project, 2000, Thermochim. Acta 387 (2002) 173–183, https://doi.org/10.1016/S0040-6031(01)00841-3.